

# A concise reference to (projected) Sérsic $R^{1/n}$ quantities, including Concentration, Profile Slopes, Petrosian indices, and Kron Magnitudes

Alister W. Graham<sup>A,B</sup> and Simon P. Driver<sup>A</sup>

<sup>A</sup> Mount Stromlo and Siding Spring Observatories, Australian National University, Private Bag, Weston Creek PO, ACT 2611, Australia.

<sup>B</sup> Email: Graham@mso.anu.edu.au

**Abstract:** Given the growing use of Sérsic’s (1963, 1968)  $R^{1/n}$  model for describing the stellar distributions in galaxies, and the lack of any single reference that provides the various associated mathematical expressions, we have endeavoured to compile such a resource here. We present the standard intensity profile, and its various guises such as the luminosity, surface–brightness, and aperture–magnitude profile. Expressions to transform the effective surface brightness into the mean effective and central surface brightness are also given, as is the expression to transform between effective radii and exponential scale–lengths. We additionally provide expressions for deriving the ‘concentration’ of an  $R^{1/n}$  profile, and two useful equations for the logarithmic slope of the light–profile are given. Petrosian radii and fluxes are also derived for a range of Sérsic profiles and compared with the effective radii and total flux. Similarly, expressions to obtain Kron radii and fluxes are presented as a function of the Sérsic index  $n$  and the number of effective radii sampled. Illustrative figures are provided throughout. Finally, the core–Sérsic model, consisting of an inner power–law and an outer–Sérsic function, is presented.

**Keywords:** galaxies: structure, galaxies: fundamental parameters, methods: analytical, methods: data analysis

## 1 Introduction

Working with the 30-inch Reynolds telescope<sup>1</sup> at what was then Australia’s Commonwealth Observatory, and today known as Mount Stromlo Observatory, Gérard de Vaucouleurs published in 1956 the most extensive southern galaxy Atlas of the day. In the following year, José Luis Sérsic commenced work at the 1.54-m telescope at the Astrophysical Station at Bosque Alegre in Argentina. His studies from 1957–1966 culminated in his 1968 southern–hemisphere galaxy Atlas ‘Galaxias Australes’. It too has proven an invaluable contribution to our understanding of galaxies, evidenced by its status as a top 1000 cited astronomy publication.

In the Introduction of Sérsic’s Atlas, it not only states the merits for a visual representation of galaxies, but, like de Vaucouleurs’, it stresses the necessity to go beyond this and obtain quantitative measures of the light distribution. This was not mere rhetoric as his Atlas consists of two parts, one pictorial in nature and the latter quantitative. It is apparent that his generalisation of de Vaucouleurs’ (1948, 1959)  $R^{1/4}$  model to an  $R^{1/n}$  model was not merely something he mentioned in passing, but something which he felt *should* be done. Indeed, Sérsic fitted the  $R^{1/n}$  model to every (sufficiently large) galaxy in his Atlas. He derived expressions to compute total (extrapolated) galaxy magnitudes, provided tables of assorted structural param-

eters associated with the  $R^{1/n}$  model, and showed how they correlated with galaxy morphological type (his Figure 3) and galaxy concentration (his Figure 4, page 145). Sérsic (1963) even provides a prescription to correct the  $R^{1/n}$  model parameters for Gaussian seeing due to atmospheric and instrumental dispersion.

It is, however, of interest to note that Sérsic’s conviction lay in the observation that different galaxies possessed differing degrees of an  $R^{1/4}$  bulge and an  $R^{1/1}$  disk component. This mixture of bulge and disk components produces a combined surface brightness profile with an intermediary form, hence the  $R^{1/n}$  model.

Today, usually when the required resolution is lacking to properly decompose an image into its separate bulge and disk components, galaxies are modelled with a single  $R^{1/n}$  profile, just as Sérsic proposed (e.g., Blanton et al. 2003). While such an approach certainly has its merits, we now know that dynamically hot stellar systems themselves possess a range of profile shapes that are well described with the  $R^{1/n}$  model (e.g., Graham & Guzmán 2003, and references therein). Detailed studies of well resolved lenticular and disk galaxies are routinely fitted with the combination of an exponential–disk plus an  $R^{1/n}$ –bulge (e.g., Andredakis, Peletier, & Balcells 1995; Seigar & James 1998; Iodice, D’Onofrio, & Capaccioli 1997, 1999; Khosroshahi, Wadadekar, & Kembhavi 2000; D’Onofrio 2001; Graham 2001a; Möllenhoff & Heidt 2001). In either case, since the work of Capaccioli in the late 1980s and in particular Caon, Capaccioli, & D’Onofrio

<sup>1</sup>The Reynolds telescope was sadly destroyed in the 2003 Canberra bush fires.

(1993) and D’Onofrio, Capaccioli, & Caon (1994), the past decade has seen an explosion in the application of the  $R^{1/n}$  model (e.g., Cellone, Forte, & Geisler 1994; Vennik & Richter 1994; Young & Currie 1994, 1995; Graham et al. 1996; Karachentseva 1996, Vennik et al. 1996, to mention just a few early papers), yet no single resource exists for the expressions and quantities pertaining to the  $R^{1/n}$  model. Moreover, no one reference provides more than a few of the relevant equations, and many textbooks still only refer to the  $R^{1/4}$  model.

This (largely review) article intends to provide a compendium of equations, numbers, and figures for ease of reference. The derivation of these also provide useful exercises for students. Where appropriate, we have endeavoured to cite the first, or at least a useful early, reference to any given equation. To the best of our knowledge, Figures (6) through (10), describing Petrosian indices and Kron magnitudes, have never been seen before. A brief reference to where readers can find deprojected expressions, and how to deal with practical issues such as seeing, is given at the end. No attempt has been made here to show the numerous scientific advances engendered via application of the  $R^{1/n}$  model.

## 2 Sérsic related quantities

### 2.1 The Sérsic profile

Sérsic’s (1963; 1968)  $R^{1/n}$  model is most commonly expressed as an intensity profile, such that

$$I(R) = I_e \exp \left\{ -b_n \left[ \left( \frac{R}{R_e} \right)^{1/n} - 1 \right] \right\}, \quad (1)$$

where  $I_e$  is the intensity at the effective radius  $R_e$  that encloses half of the total light from the model (Caon et al. 1993; see also Ciotti 1991, his Equation 1). The constant  $b_n$  is defined in terms of the third and final parameter  $n$  which describes the ‘shape’ of the light-profile, and is given below.<sup>2</sup>

One can integrate Equation (1) over a projected area  $A = \pi R^2$  to obtain the luminosity,  $L$ , interior to any radius  $R$ . This is simply a matter of solving the integral<sup>3</sup>

$$L(< R) = \int_0^R I(R') 2\pi R' dR',$$

which yields, after substituting in  $x = b_n (R/R_e)^{1/n}$ ,

$$L(< R) = I_e R_e^2 2\pi n \frac{e^{b_n}}{(b_n)^{2n}} \gamma(2n, x), \quad (2)$$

<sup>2</sup>It is common for researchers studying dwarf galaxies to replace the exponent  $1/n$  with  $n$ . In this case, de Vaucouleurs’ model would have  $n = 0.25$ , rather than 4.

<sup>3</sup>Obviously if one is using a major- or minor-axis profile, rather than the geometric mean ( $R = \sqrt{ab}$ ) profile, an ellipticity term will be required. This is trivial to add and for the sake of simplicity won’t be included here. The issue of ellipticity gradients is more difficult, and interested readers should look at Ferrari et al. (2004).

where  $\gamma(2n, x)$  is the incomplete gamma function defined by

$$\gamma(2n, x) = \int_0^x e^{-t} t^{2n-1} dt. \quad (3)$$

Replacing  $\gamma(2n, x)$  with  $\Gamma(2n)$  in Equation (2) gives one the value of  $L_{tot}$  (Ciotti 1991).

Thus, the value of  $b_n$  which we saw in Equation (1) is such that

$$\Gamma(2n) = 2\gamma(2n, b_n), \quad (4)$$

where  $\Gamma$  is the (complete) gamma function (Ciotti 1991). Common values of  $b_n$  are  $b_4 = 7.669$  and  $b_1 = 1.678$ . In passing we note a useful property of the  $\Gamma$  function, which is,  $\Gamma(2n) = (2n - 1)!$ .

Analytical expressions which approximate the value of  $b_n$  have been developed. Capaccioli (1989) provided one of the first such approximations such that  $b_n = 1.9992n - 0.3271$ , for  $0.5 < n < 10$  (see also Prugniel & Simien 1997, their equation A3a). Ciotti & Bertin (1999) showed  $b_n \rightarrow 2n - 1/3$  for large values of  $n$ , and in practice this provides a better fit for values of  $n$  greater than about 8 (see Graham 2001a, his Figure 2). Ciotti & Bertin (1999) also provided an asymptotic expansion which, for values of  $n > 0.36$ , is accurate to better than  $10^{-4}$  and the approximation of choice. For smaller values of  $n$ , MacArthur, Courteau, & Holtzman (2003) provide a fourth order polynomial which is accurate to better than two parts in  $10^3$  (see their Figure 23). However, the exact value of  $b_n$  in Equation (4) can be solved numerically, and fast codes exist to do this,

For an exponential ( $n = 1$ ) profile, 99.1% of the flux resides within the inner  $4 R_e$  (90.8% within the inner 4 scale-lengths) and 99.8% of the flux resides within the inner  $5 R_e$  (96.0% within the inner 5 scale-lengths). For an  $n = 4$  profile, 84.7% of the flux resides within the inner  $4 R_e$  and 88.4% within the inner  $5 R_e$ .

Multiplying the negative logarithm of the luminosity profile (Equation 2) by 2.5 gives the enclosed magnitude profile, known as the ‘curve of growth’,

$$m(< R) = \mu_e - 5 \log R_e - 2.5 \log \left[ 2\pi n \frac{e^{b_n}}{(b_n)^{2n}} \gamma(2n, x) \right], \quad (5)$$

which asymptotes to the total apparent magnitude  $m_{tot}$  as  $R$  tends to infinity and, consequently,  $\gamma(2n, x) \rightarrow \Gamma(2n)$  (Figure 1).

Multiplying the negative logarithm of Equation (1) by 2.5 yields the surface brightness profile (Figure 1), as used in Caon et al. (1993),

$$\mu(R) = \mu_e + \frac{2.5b_n}{\ln(10)} \left[ (R/R_e)^{1/n} - 1 \right]. \quad (6)$$

#### 2.1.1 Asymptotic behavior for large $n$

For large values of  $n$ , the Sérsic model tends to a power-law with slope equal to 5. Substituting  $e^t = z = R/R_e$  into Equation (1), one has

$$I(z) \sim \exp \left\{ -b_n \left[ e^{t/n} - 1 \right] \right\}.$$

Now, for large  $n$ ,  $e^{t/n}$  is small, and so one can use  $e^{t/n} \sim 1 + t/n$ . One can also use  $b_n \sim 2n$  to give

$$\ln[I(z)] \sim -b_n [t/n] \sim -2t \sim -2 \ln(z).$$

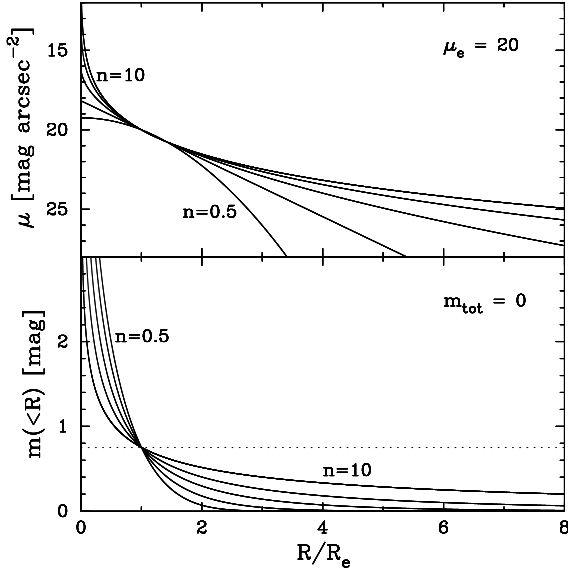


Figure 1: Top panel: Sérsic surface brightness profiles (Equation 6) for  $n=0.5, 1, 2, 4,$  and  $10$ . The profiles have been normalised at  $\mu_e = 20$  mag arcsec $^{-2}$ . Bottom panel: Sérsic aperture magnitude profiles (Equation 5), normalised such that the total magnitude equals zero. The dotted line is offset by  $0.75$  mag (a factor of  $2$  in flux) from the total magnitude.

Thus  $\mu(z) = -2.5 \log[I(z)] \sim 5 \log(z)$ .

For simplicity, the subscript ‘ $n$ ’ will be dropped from the term  $b_n$  in what follows.

## 2.2 Surface brightness, radial scale, and absolute magnitude

From the value of  $\mu_e$ , the ‘effective surface brightness’ at  $R_e$ , and knowing the value of  $n$ , one can compute both the central surface brightness  $\mu_0$  and the average/mean surface brightness  $\langle \mu \rangle_e$  within the effective radius.

At the centre of the profile one has, from Equation (6),

$$\begin{aligned} \mu(R=0) &\equiv \mu_0 = \mu_e - 2.5b/\ln(10), & (7) \\ \mu_0 &= \mu_e - 1.822, n = 1, \\ \mu_0 &= \mu_e - 8.327, n = 4. \end{aligned}$$

The difference between  $\mu_e$  and  $\mu_0$  is shown in Figure (2) as a function of the Sérsic index  $n$ .

The ‘mean effective surface brightness’, often simply referred to as the ‘mean surface brightness’, is computed as follows. The average intensity,  $\langle I \rangle_e$ , within the effective radius is obtained by integrating the intensity over the area  $A = \pi R_e^2$  such that

$$\langle I \rangle_e = \frac{\int I dA}{A} = \frac{I_e e^b \int_0^{R_e} e^{-b(R/R_e)^{1/n}} 2\pi R dR}{\pi R_e^2}.$$

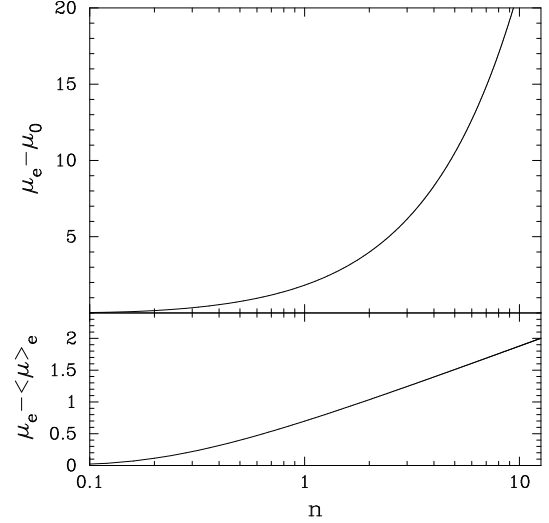


Figure 2: Top panel: Difference between the central surface brightness  $\mu_0$  and the effective surface brightness  $\mu_e$  as a function of profile shape  $n$ . Bottom panel: Difference between  $\mu_e$  and the mean effective surface brightness  $\langle \mu \rangle_e$  as a function of  $n$ .

Letting  $x = b(R/R_e)^{1/n}$ , one has

$$\langle I \rangle_e = I_e f(n),$$

where

$$f(n) = \frac{2ne^b}{b^{2n}} \int_0^b e^{-x} x^{2n-1} dx.$$

Now as  $b$  was chosen such that  $R_e$  is the radius containing half of the total light, one has

$$f(n) = \frac{ne^b}{b^{2n}} \int_0^\infty e^{-x} x^{2n-1} dx = \frac{ne^b}{b^{2n}} \Gamma(2n). \quad (8)$$

Thus,

$$\begin{aligned} \langle \mu \rangle_e &= \mu_e - 2.5 \log[f(n)], & (9) \\ \langle \mu \rangle_e &= \mu_e - 0.699, n = 1, \\ \langle \mu \rangle_e &= \mu_e - 1.393, n = 4. \end{aligned}$$

The difference between  $\mu_e$  and  $\langle \mu \rangle_e$  is shown in Figure (2) as a function of the Sérsic index  $n$  (Caon et al. 1994; Graham & Colless 1997).

Substituting equation 9 into Equation 5, one has, at  $R = R_e$ ,

$$m(< R_e) = \langle \mu \rangle_e - 2.5 \log(\pi R_e^2), \quad (10)$$

and thus<sup>4</sup>

$$m_{\text{tot}} = \langle \mu \rangle_e - 2.5 \log(2\pi R_e^2), \quad (11)$$

<sup>4</sup>Using empirical measurements within some suitably large aperture, one has from simple geometry that  $\langle \mu \rangle_{1/2} = m_{\text{tot,ap}} + 2.5 \log(2\pi R_{1/2}^2)$ . Expressions to correct these approximate values — due to the missed flux outside of one’s chosen aperture — are given in Graham et al. (2005).

This expression can be rewritten in terms of the absolute magnitude,  $M_{\text{tot}}$ , the effective radius in kpc,  $R_{e,\text{kpc}}$ , and the *absolute* effective surface brightness,  $\langle\mu\rangle_{e,\text{abs}}$ , (i.e., the mean effective surface brightness if the galaxy was at a distance of 10pc):

$$M_{\text{tot}} = \langle\mu\rangle_{e,\text{abs}} - 2.5 \log(2\pi R_{e,\text{kpc}}^2) - 2.5 \log \left[ \left( \frac{360 \times 60 \times 60}{2\pi \times 0.01} \right)^2 \right],$$

$$M_{\text{tot}} = \langle\mu\rangle_{e,\text{abs}} - 2.5 \log(2\pi R_{e,\text{kpc}}^2) - 36.57 \quad (12)$$

The apparent and absolute mean effective surface brightnesses are related by the cosmological corrections:

$$\langle\mu\rangle_{e,\text{abs}} = \langle\mu\rangle_e - 10 \log(1+z) - E(z) - K(z), \quad (13)$$

where  $z$ ,  $E(z)$ , and  $K(z)$  are the redshift, evolutionary correction, and K-correction respectively (e.g., Driver et al. 1994 and references therein).

Another transformation arises from the use of scale-lengths  $h$  rather than effective radii  $R_e$ . When the  $R^{1/n}$  model is written as

$$I(R) = I_0 \exp \left[ -(R/h)^{1/n} \right] \quad (14)$$

(e.g., Ellis & Perry 1979, their page 362; Davies et al. 1988), where  $I_0 = I(R=0)$ , one has

$$I_0 = I_e e^b, \quad (15)$$

$$R_e = b^n h, \quad (16)$$

$$R_e = 1.678h, n = 1,$$

$$R_e = 3466h, n = 4.$$

It's straightforward to show that

$$\mu(R) = \mu_0 + \frac{2.5}{\ln(10)} \left( \frac{R}{h} \right)^{1/n}, \quad (17)$$

$$\mu(R) = \mu_0 + 1.086(R/h), n = 1,$$

and

$$L_{\text{tot}} = \pi I_0 h^2 \Gamma(2n+1). \quad (18)$$

Given the small scale-lengths associated with the  $n = 4$  model, and the practical uncertainties in deriving a galaxy's central brightness, one can appreciate why Equation (1) is preferred over Equation (14).

If one is modelling a two-component spiral galaxy, consisting of an exponential disk and an  $R^{1/n}$  bulge, then the bulge-to-disk luminosity ratio is given by the expression

$$\frac{B}{D} = \frac{n\Gamma(2n)e^b}{b^{2n}} \left( \frac{R_e^2}{h^2} \right) \left( \frac{I_e}{I_0} \right), \quad (19)$$

where  $h$  and  $I_0$  are respectively the scale-length and central intensity of the disk, and  $R_e$ ,  $I_e$ , and  $n$  describe the Sérsic bulge profile. Noting that  $2n\Gamma(2n) = \Gamma(2n+1) = (2n)!$ , the above equation can be simplified for integer values of  $2n$ . For those who are curious, the first term on the right hand side of the equality can be seen plotted as a function of  $n$  in Graham (2001a).

## 2.3 Concentration

For many years astronomers have had an interest in how centrally concentrated a galaxy's stellar distribution is (e.g., Morgan 1958, 1959, 1962; Fraser 1972; de Vaucouleurs 1977). Sérsic (1968) used de Vaucouleurs (1956) somewhat subjective size ratio between the main region of the galaxy and the apparent maximum dimension of the galaxy as a measure of concentration.

Trujillo, Graham & Caon (2001c) defined a useful, objective expression for concentration, such that, in pixelated form

$$C_{R_e}(\alpha) = \frac{\sum_{i,j \in E(\alpha R_e)} I_{ij}}{\sum_{i,j \in E(R_e)} I_{ij}}. \quad (20)$$

Here,  $E(R_e)$  means the isophote which encloses half of the total light, and  $E(\alpha R_e)$  is the isophote at a radius  $\alpha$  ( $0 < \alpha < 1$ ) times  $R_e$ . This is a flux ratio. For a Sérsic profile which extends to infinity,

$$C_{R_e}(\alpha) = \frac{\gamma(2n, b\alpha^{1/n})}{\gamma(2n, b)}. \quad (21)$$

This expression is a monotonically increasing function of  $n$ , and for  $\alpha = 1/3$  it's values are shown in Figure (3). An often unrealized point is that if every elliptical galaxy had an  $R^{1/4}$  profile then they would all have exactly the same degree of concentration. Observational errors aside, it is only because elliptical galaxy light-profiles deviate from the  $R^{1/4}$  model that a range of concentrations exist. This is true for all objective concentration indices in use today.

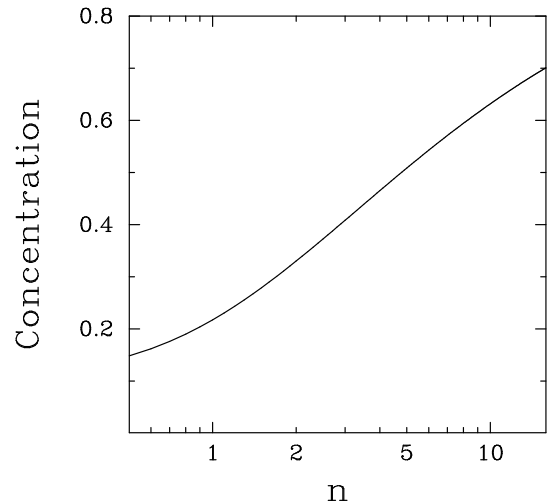


Figure 3: The central concentration  $C_{R_e}(1/3)$ , as defined by Trujillo et al. (2001c), is a monotonically increasing function of the Sérsic index  $n$ .

It should be noted that astronomers don't actually know where the edges of elliptical galaxies occur; their light-profiles appear to peter-out into the background noise of the sky. Due to the presence of faint, high-redshift galaxies and scattered light, it is

not possible to determine the sky-background to an infinite degree of accuracy. From an analysis of such sky-background noise sources, Dalcanton & Bernstein (2000, see also Capaccioli & de Vaucouleurs 1983) determined the limiting surface brightness threshold to be  $\mu \sim 29.5$   $B$ -mag arcsec $^{-2}$  and  $\mu \sim 29$   $R$ -mag arcsec $^{-2}$ . Such depths are practically never achieved and shallow exposures often fail to include a significant fraction of an elliptical galaxy's light. One would therefore like to know how the concentration index may vary when different galaxy radial extents are sampled but no effort is made to account for the missed galaxy flux. The resultant impact on  $C_{R_e}$  and other popular concentration indices is addressed in Graham, Trujillo, & Caon (2001).

It was actually, in part, because of the unstable nature of the popular concentration indices that Trujillo et al. (2001c) introduced the notably more stable index given in Equations (20) and (21). The other reason was because the concentration index  $C(\alpha) = \sum_{i,j \in E(\alpha)} I_{ij} / \sum_{i,j \in E(1)} I_{ij}$ , where  $E(\alpha)$  denotes some inner radius which is  $\alpha$  ( $0 < \alpha < 1$ ) times the outermost radius which has been normalized to 1 (Okamura, Kodaira, & Watanabe 1984; Doi, Fukugita, & Okamura 1993; Abraham et al. 1994), should tend to 1 for practically every profile that is sampled to a large enough radius. It is only because of measurement errors, undersampling, or the presence of truncated profiles such as the exponential disks in spiral galaxies, that this index deviates from a value of 1.

## 2.4 Profile slopes

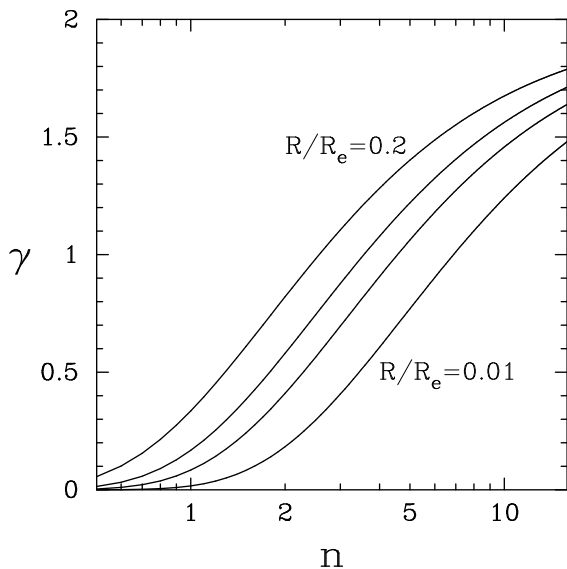


Figure 4: The slope of the Sérsic profile  $\gamma$  (Equation 23) is shown as a function of profile shape  $n$  for  $R/R_e=0.01, 0.05, 0.1,$  and  $0.2$ .

Given *HST*'s ability to resolve the inner light-profiles of nearby galaxies, the slope  $\gamma$  of a galaxy's nuclear

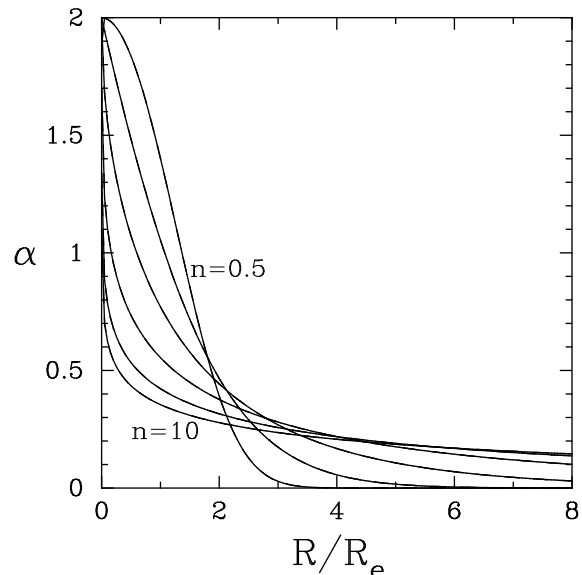


Figure 5: The slope  $\alpha$  (Equation 25) is shown as a function of normalised radius  $R/R_e$  for  $n=0.5, 1, 2, 4, 7,$  and  $10$ .

(the inner few hundred parsec) stellar distribution has become a quantity of interest. Defining<sup>5</sup>

$$\gamma(R) \equiv \frac{-d[\log I(R)]}{d \log R}, \quad (22)$$

Rest et al. (2001, their Equation 8) used this to measure the nuclear slopes of 'core' and 'power-law' galaxies. From Equation (1) one can obtain

$$\gamma(R, n) = (b/n)(R/R_e)^{1/n}. \quad (23)$$

This is approximately  $2(R/R_e)^{1/n}$  (see section 2.1). Thus, at constant  $(R/R_e)$ ,  $\gamma$  is a monotonically increasing function of the Sérsic index  $n$  (Graham et al. 2003b).

It turns out Equation (23) is appropriate for the so-called 'power-law' galaxies which are now known to possess Sérsic profiles down to their resolution limit (Trujillo et al. 2004) and would be better referred to as 'Sérsic' galaxies as they do not have power-law profiles. A modification is however required for the luminous 'core galaxies', and is described in Section 2.7.

Another logarithmic slope of interest is that used by Gunn & Oke (1975) and Hoessel (1980), and is defined as

$$\alpha(R) \equiv \frac{d[\ln L(R)]}{d \ln R}. \quad (24)$$

From Equation (2) one has

$$\alpha(x, n) = \frac{x}{nL(x)} \frac{d[L(x)]}{dx} = \frac{e^{-x} x^{2n}}{n\gamma(2n, x)}, \quad (25)$$

where, as before,  $x = b(R/R_e)^{1/n}$  (Graham et al. 1996, their equation 8).

<sup>5</sup>This  $\gamma$  should not be confused with the incomplete gamma function seen in Equation (3).

Figures (4) and (5) show how  $\gamma(R)$  and  $\alpha(R)$  vary with normalised radius  $R/R_e$  for a range of different profile shapes  $n$ .

## 2.5 Petrosian index and magnitude

The Petrosian (1976, his Equation 7) function  $\eta(R)$  is given as

$$\eta(R) = \frac{2\pi \int_0^R I(R')R'dR'}{\pi R^2 I(R)}, \quad (26)$$

$$= \frac{L(< R)}{\pi R^2 I(R)} = \frac{\langle I \rangle_R}{I(R)}. \quad (27)$$

It is the average intensity within some projected radius  $R$  divided by the intensity at that radius. The logarithmic expression is written as

$$2.5 \log[\eta(R)] = \mu(R) - \langle \mu \rangle_R, \quad (28)$$

and is shown in Figure (6) for a range of profile shapes  $n$ .

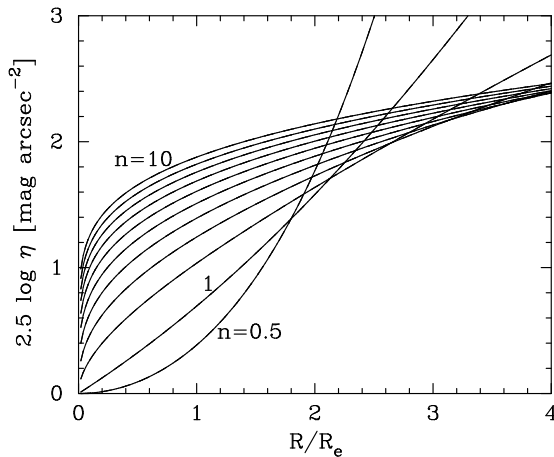


Figure 6: The logarithm of the Petrosian function  $\eta(R)$  (Equation 28) is shown as a function of normalised radius  $R/R_e$  for Sérsic profiles having  $n=0.5, 1, 2, 3, \dots, 10$ .

This is a particular clever quantity because if every galaxy had the same stellar distribution, such as an  $R^{1/4}$  profile, then a radius where the  $\eta$ -function equalled some pre-defined, constant value would correspond to the same number of  $R_e$  for every galaxy. Moreover, such measurements are unaffected by such things as exposure-depth, galactic dust, and cosmological redshift dimming because they affect both surface brightness terms in Equation (28) equally. Even though it is possible to measure the Petrosian radius without ever assuming or specifying an underlying light-profile model, the actual form of the stellar distribution is implicitly incorporated into the Petrosian function and so cannot be ignored (as Figure 6 reveals).

It turns out the Petrosian function is equal to

$$\eta(R) = 2/\alpha(R), \quad (29)$$

where  $\alpha(R)$  is given in Equation (24; Djorgovski & Spinrad 1981; Djorgovski, Spinrad & Marr 1984; Sandage & Perelmuter 1990, their Section IIa; Kjærgaard, Jørgensen, & Moles 1993). Thus

$$\eta(x, n) = \frac{2n\gamma(2n, x)}{e^{-x}x^{2n}}. \quad (30)$$

The flux within twice the radius  $R_P$  when  $1/\eta(R_P) = 0.2$  is often used to estimate an object's flux (e.g., Bershady, Jangren, & Conselice 2000; Blanton et al. 2001), as is the flux within  $3R_P$  when  $1/\eta(R_P) = 0.5$  (e.g., Conselice, Gallagher, & Wyse 2002; Conselice et al. 2003). How well this works of course depends on the shape of the light-profile, and Figure (7) shows these approximations to the total luminosity as a function of the Sérsic index  $n$ . In the case of  $2R_P$  when  $1/\eta(R_P) = 0.2$ , one can see that profiles with  $n=10$  will have their luminosities under-estimated by 44.7% and those with  $n=4$  by only 17.1%. The situation is considerably worse when using  $3R_P$  and  $1/\eta(R_P) = 0.5$ . A prescription to correct for the missing light, beyond one's chosen aperture, is detailed in Graham et al. (2005).

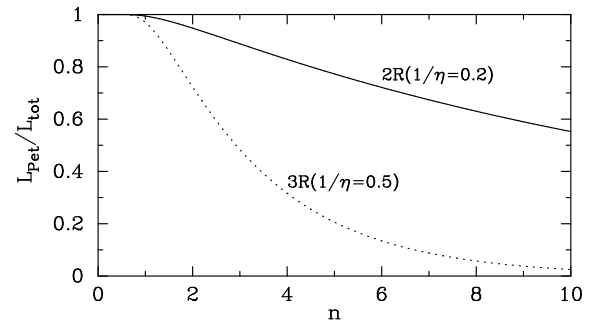


Figure 7: Flux ratio, as a function of light-profile shape  $n$ , between the total luminosity  $L_{\text{tot}}$  and the Petrosian luminosity  $L_{\text{Pet}}$  inside (i) twice the radius  $R_P$  where  $1/\eta(R_P) = 0.2$  (solid curve) and (ii) thrice the radius  $R_P$  where  $1/\eta(R_P) = 0.5$  (dotted curve).

## 2.6 Kron magnitudes

Kron (1980) presented the following luminosity-weighted radius,  $R_1$ , which defines the ‘first moment’ of an image

$$R_1(R) = \frac{2\pi \int_0^R I(x)x^2 dx}{2\pi \int_0^R I(x)x dx}. \quad (31)$$

He argued that an aperture of radius twice  $R_1$ , when  $R_1$  is obtained by integrating to a radius  $R$  that is 1% of the sky flux, contains more than  $\sim 90\%$  of an object's total light, making it a useful tool for estimating an object's flux.

It is worth noting that considerable confusion exists in the literature in regard to the definition of  $R_1$ . To help avoid ambiguity, we point out that  $g(x)$  in Kron's (1980) original equation refers to  $xI(x)$ , where

$x$  is the radius and  $I(x)$  the intensity profile. Infante (1987) followed this notation, but confusingly a typo appears immediately after his Equation 3 where he has written  $g(x) \sim I(x)$  instead of  $g(x) \sim xI(x)$ . Furthermore, Equation 3 of Bertin & Arnouts (1996) is given as  $R_1 = \sum RI(R) / \sum I(R)$  where the summation is over a two-dimensional aperture rather than a one-dimensional light-profile. In the latter case, one would have  $R_1 = \sum R^2 I(R) / \sum RI(R)$ .

Using a Sérsic intensity profile, and substituting in  $x = b(R/R_e)^{1/n}$ , the numerator can be written as

$$2\pi n I_e e^b R_e^3 \gamma(3n, x) / b^{3n}.$$

Using Equation (2) for the denominator, which is simply the enclosed luminosity, Equation (31) simplifies to

$$R_1(x, n) = \frac{R_e \gamma(3n, x)}{b^n \gamma(2n, x)}. \quad (32)$$

The use of ‘Kron radii’ to determine ‘Kron magnitudes’ has proved very popular, and SExtractor (Bertin & Arnouts 1996) obtains its magnitudes using apertures that are 2.5 times  $R_1$ . Recently, however, it has been reported that such an approach may, in some instances, be missing up to half of a galaxy’s light (Bernstein, Freedman, & Madore 2002; Benitez et al. 2004). If the total light is understood to be that coming from the integration to infinity of a light-profile, then what is important is not the sky-level or isophotal-level one reaches, but the number of effective radii that have been sampled.

For a range of light-profile shapes  $n$ , Figure (8) shows the value of  $R_1$  (in units of  $R_e$ ) as a function of the number of effective radii to which Equation (31) has been integrated. Given that one usually only measures a light-profile out to 3–4  $R_e$  at best, one can see that only for light-profiles with  $n$  less than about 1 will one come close to the asymptotic value of  $R_1$  (i.e. the value obtained if the profile was integrated to infinity). Table (1) shows these asymptotic values of  $R_1$  as a function of  $n$ , and the magnitude enclosed within  $2R_1$  and  $2.5R_1$ . This is, however, largely academic because observationally derived values of  $R_1$  will be smaller than those given in Table (1), at least for light-profiles with values of  $n$  greater than about 1.

Table 1: Theoretical Kron Radii and Magnitudes

Sérsic $n$	$R_1$ [ $R_e$ ]	$L(< 2R_1)$ %	$L(< 2.5R_1)$ %
0.5	1.06	95.7	99.3
1.0	1.19	90.8	96.0
2.0	1.48	87.5	92.2
3.0	1.84	86.9	90.8
4.0	2.29	87.0	90.4
5.0	2.84	87.5	90.5
6.0	3.53	88.1	90.7
7.0	4.38	88.7	91.0
8.0	5.44	89.3	91.4
9.0	6.76	90.0	91.9
10.0	8.39	90.6	92.3

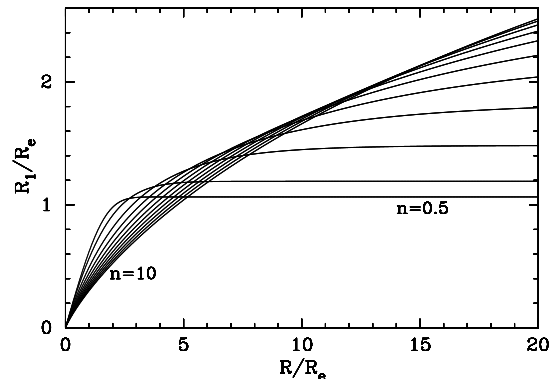


Figure 8: Kron radii  $R_1$ , as obtained from Equation (32), are shown as a function of the radius  $R$  to which the integration was performed. Values of  $n$  range from 0.5, 1, 2, 3, ... 10.

From Figure (8) one can see, for example, that an  $R^{1/4}$  profile integrated to  $4R_e$  will have  $R_1 = 1.09R_e$  rather than the asymptotic value of  $2.29R_e$ . Now  $2.5 \times 1.09R_e$  encloses 76.6% of the object’s light rather than 90.4% (see Table 1). This is illustrated in Figure (9) where one can see when and how Kron magnitudes fail to represent the total light of an object. This short-coming is worse when dealing with shallow images and with highly concentrated systems having large values of  $n$  (brightest cluster galaxies are known to have Sérsic indices around 10 or greater, Graham et al. 1996).

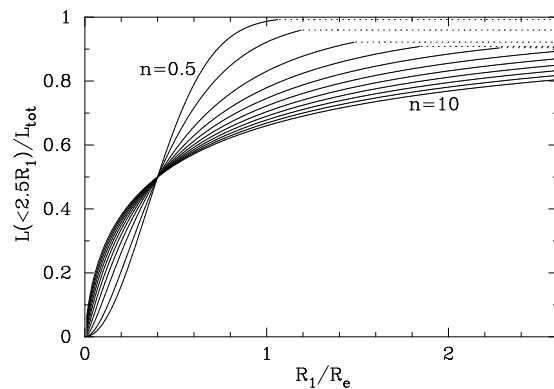


Figure 9: Kron luminosity within  $2.5R_1$ , normalised against the total luminosity, as a function of how many effective radii  $R_1$  corresponds to. Values of  $n$  range from 0.5, 1, 2, 3, ... 10.

To provide a better idea of the flux fraction represented by Kron magnitudes, and one which is more comparable with Figure (7), Figure (10) shows this fraction as a function of light-profile shape  $n$ . The different curves result from integrating Equation (31) to different numbers of effective radii in order to obtain  $R_1$ . If  $n=4$ , for example, but one only integrates out to  $1R_e$  (where  $R_e$  is again understood to be the true, intrinsic value rather than the observed value), then

the value of  $R_1$  is  $0.41R_e$  and the enclosed flux within  $2.5R_1$  is only 50.7%. If an  $n=10$  profile is integrated to only  $1R_e$ , then  $R_1=0.30R_e$  and the enclosed flux is only 45.0% within  $2.5R_1$ . It is therefore easy to understand why people have reported Kron magnitudes as having missed half of an object’s light.

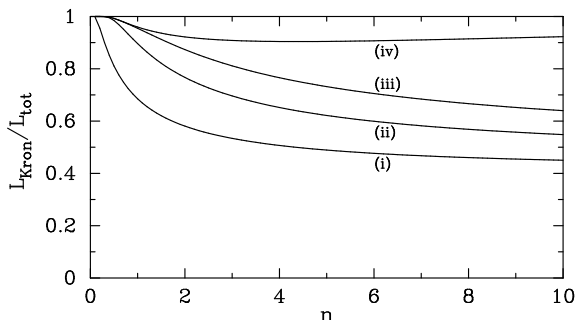


Figure 10: Kron luminosity within  $2.5R_1$ , normalised against the total luminosity, as a function of the underlying light–profile shape  $n$ . The different curves arise from the different values of  $R_1$  obtained by integrating Equation (31) to (i)  $1R_e$ , (ii)  $2R_e$ , (iii)  $4R_e$ , and (iv) infinity.

## 2.7 The core–Sérsic model

Due to the presence of partially depleted cores in luminous ( $M_B < -20.5$  mag,  $H_0 = 70$  km s $^{-1}$  Mpc $^{-1}$ ) elliptical galaxies<sup>6</sup>, a ‘core–Sérsic’ model (Graham et al. 2003a,b) has been developed in order to describe and connect the nuclear (typically less than a few hundred parsecs) and the remaining outer stellar distribution. This model consists of an inner power–law and an outer Sérsic function, and has proven essential for modeling the *HST*–resolved light–profiles of luminous early–type galaxies (Trujillo et al. 2004). As suggested in Graham et al. (2003b), the lower–luminosity ‘power–law’ galaxies have been shown to be described by the Sérsic model over their entire radial extent (Trujillo et al. 2004).

Although the reader is referred to the above papers, especially the Appendix of Trujillo et al. (2004), the core–Sérsic model is given as<sup>7</sup>:

$$I(R) = I' \left[ 1 + \left( \frac{R_b}{R} \right)^\alpha \right]^{\gamma/\alpha} \exp \left\{ -b \left[ (R^\alpha + R_b^\alpha) / R_e^\alpha \right]^{1/(\alpha n)} \right\} \quad (33)$$

<sup>6</sup>The luminous ‘core galaxies’ likely correspond to the ‘bright’ family of galaxies identified in Capaccioli, Caon, & D’Onofrio et al. (1992) and Caon et al. (1993). They tend to have boxy rather than disk isophotes (Nieto et al. 1991), and Sérsic indices greater than  $\sim 4$ . They are commonly understood to be the product of (elliptical) galaxy mergers (e.g., Capaccioli, Caon, & D’Onofrio 1992, 1994; Graham 2004)

<sup>7</sup>The  $\alpha$  and  $\gamma$  terms shown here should not be confused with those given earlier in the paper, they are different quantities.

where  $R_b$  is the break–radius separating the inner power–law having logarithmic slope  $\gamma$  from the outer Sérsic function. The intensity  $I_b$  at the break–radius  $R_b$  can be evaluated from the expression

$$I' = I_b 2^{-(\gamma/\alpha)} \exp \left[ b(2^{1/\alpha} R_b / R_e)^{1/n} \right]. \quad (34)$$

The final parameter,  $\alpha$ , controls the sharpness of the transition between the inner (power–law) and outer (Sérsic) regimes — higher values of  $\alpha$  indicating sharper transitions. In practice (e.g., Figure 11) we find that a sharp transition is adequate and recommend setting  $\alpha$  to a suitably large constant value (typically anything greater than 3 is fine), leaving one with a 5–parameter core–Sérsic model.

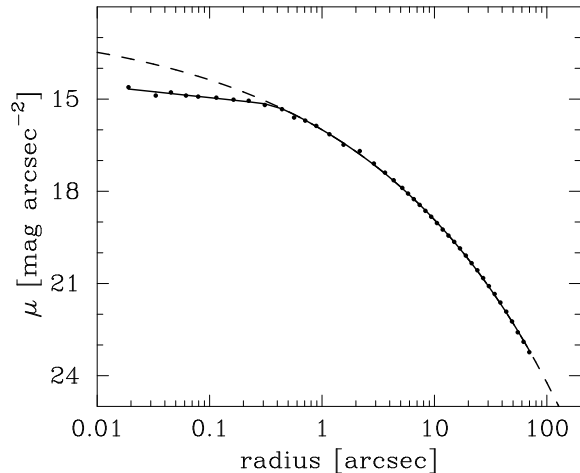


Figure 11: Major–axis, *R*–band light–profile of NGC 3348. The solid line is the best–fitting core–Sérsic model while the dashed line is the best–fitting Sérsic model to the data beyond the *HST*–resolved break radius (Graham et al. 2003a,b; Trujillo et al. 2004).

## 2.8 Deprojected quantities and dynamical terms

Ciotti (1991) provides an exact, numerical expression for the deprojected light–profile of the  $R^{1/n}$  model, that is, the luminosity density profile. He additionally provides numerical expressions for the gravitational potential and also the spatial and line–of–sight velocity dispersions. These must however be solved by integration, which means they require considerably more computer time than analytical expressions. Ciotti does however provide analytical expressions for the behavior of the above expressions at both small and large radii. Luminosity–weighted aperture velocity dispersions have been used in Ciotti, Lanzoni, & Renzini (1996), and also in Graham & Colless (1997) where the radial profiles are shown for different values of the Sérsic index  $n$ . Ciotti (1991) additionally provides expressions for the distribution function and the normalised differential energy distribution.

An exact, analytical expression for the density profile was finally discovered a couple of years ago and is given in Mazure & Capelato (2002). It involves the use of somewhat complicated Meijer G functions. For those interested in a more simple, analytical approximation, an accurate expression is given in Prugniel & Simien (1997), which is developed slightly in Lima Nieto, Gerbal, & Márquez (1999) and Trujillo et al. (2002).

Mazure & Capelato (2002) also provide exact analytical expressions for the mass, gravitational potential, total energy, and the central velocity dispersion. For modellers interested in fast-to-compute, analytical approximations for not only the density profile but also the potential and force, such expressions, which additionally include optional power-law cores, can be found elsewhere (B. Terzić & A.W. Graham, in preparation).

### 3 Sérsic magnitudes

In this article we have compiled and developed equations pertaining to the Sérsic profile in a purely analytical manner. To mention just one of many important uses of the Sérsic profile is its potential for deriving accurate total magnitudes. This need is motivated by a growing community-wide awareness of the complex nature of galaxy photometry, and in particular the large amounts of flux which can be missed by isophotal, aperture, Petrosian, or Kron magnitudes (e.g., Figures 7 & 10). Cross et al. (2004) recently compared APM, SuperCosmos, SDSS and MGC photometry for several thousand galaxies and concluded that the photometric errors are mainly dominated by the systematics of the methodology rather than the random errors. The Sérsic magnitude provides a logical standard and is derived by evaluating Equation 5 at  $R = \infty$  given  $\mu_e$ ,  $n$ , and  $R_e$  derived from a fit to the available light-profile.

In practice various “facts-of-life” issues remain; these are not specific problems to the Sérsic model, but generic to studies of galaxy photometry. The most obvious ones are: the smoothing effect of the point-spread function (PSF); profile truncation; multiple component systems; dust and asymmetric profiles. All of these can act to exacerbate or ameliorate the amount of missing flux. While a detailed discussion of these issues is beyond the scope of this paper we provide some suitable references below.

The smearing effect of the PSF will cause the observed profile to tend to  $n \approx 0.5$  (i.e., Gaussian), this is dealt with straightforwardly by incorporating PSF convolution into the model fitting process, e.g., Andredakis et al. (1995; their Equation 10) and Trujillo et al. (2001a,b). Disk truncation is trickier (see the reviews by van der Kruit (2001) and Pohlen et al. 2004) and is assumed to be related to the minimum gas density required for star-formation (Kennicutt 1989; Kregel & van der Kruit 2004). Initially truncation was reported to occur at around 4 scale-lengths for exponential disks (van der Kruit 1979; van der Kruit & Searle 1981). More recent studies have argued that the

truncation is better described by a broken exponential fit (e.g., de Grijs et al. 2001; Pohlen et al. 2002). Others argue that truncation may actually be a manifestation of poor background modelling or simply due to intrinsic variations in the disk (Narayan & Jog 2003). Certainly some recent studies find no discernible truncation to extremely faint isophotal limits; for example, NGC 300 is a pure exponential out to 10 scale-lengths (Bland-Hawthorn et al. 2005). The net result is that in practice it is not clear exactly how far out one should integrate the Sérsic profile for disk galaxies. As discussed in Section 2.3, there is no evidence for truncation in the elliptical galaxy population. From Figure 1 we see that this issue is far more significant for high Sérsic index systems. A new generation of publicly available 2D fitting codes, in particular GIM2D (Marleau & Simard 1998), GALFIT (Peng et al. 2002), and BUDDA (de Souza, Gadotti, & dos Anjos 2004), can routinely deal with multiple-component profiles. Dust opacity (Disney, Davies, & Phillipps 1989, Davies et al. 1993) can also lead to changes in the light-profile because of the more centrally concentrated dust distribution. Modelling opacity is non-trivial as there are strong inclination dependencies (Choloniewski 1991; Jones, Davies & Trewhella 1996; Graham 2001b) however models are being developed to provide detailed corrections (e.g., Pierini et al. 2004; Tuffs et al. 2004). From the dust attenuation studies of Calzetti (2001, and references therein) and many others, dust issues can be minimised via structural analysis at near-IR wavelengths. Non-biaxial asymmetry of galaxy images can be readily identified via the use of the ‘asymmetry’ measures (e.g., Schade et al. 1995; Rix & Zaritsky 1995; Conselice 1997; Kornreich, Haynes, & Lovelace 1998).

### Acknowledgments

We kindly thank Valeria Coenda for faxing us a copy of Sérsic’s 1963 article, referenced in his 1968 Atlas. We are additionally grateful to Steve Phillipps for refereeing this work, and Massimo Capaccioli for his helpful and rapid response to our request for information and references.

### References

- Abraham, R.G., Valdes, F., Yee, H.K.C., & van den Bergh, S. 1994, ApJ, 432, 75
- Andredakis, Y.C., Peletier, R.F., & Balcells, M. 1995, MNRAS, 275, 874
- Benitez, N., et al. 2004, ApJS, 150, 1
- Bernstein, R.A., Freedman, W.L., & Madore, B.F. 2002, 571, 107
- Bershad, M.A., Jangren, A., & Conselice, C.J. 2000, AJ, 119, 2645
- Bertin, E., & Arnouts, S. 1996, A&AS, 117, 393

- Bland-Hawthorn, J., Vlajić, M., Freeman, K.C., & Drain, B.T. 2005, *AJ*, submitted
- Blanton, M.R., et al. 2001, *AJ*, 121, 2358
- Blanton, M.R., et al. 2003, *ApJ*, 594, 186
- Calzetti, D. 2001, *PASP*, 113, 1449
- Caon, N., Capaccioli, M., & D'Onofrio, M. 1993, *MNRAS*, 265, 1013
- Caon, N., Capaccioli, M., D'Onofrio, M., & Longo, G. 1994, *A&A*, 286, 39
- Capaccioli, M. 1989, in *The World of Galaxies*, ed. H. G. Corwin, L. Bottinelli (Berlin: Springer-Verlag), 208
- Capaccioli, M., Caon, N., & D'Onofrio, M. 1992, *MNRAS*, 259, 323
- Capaccioli, M., Caon, N., & D'Onofrio, M. 1994, *Mem. della Societa Astronomia Italiana*, 65, 919
- Capaccioli, M., & de Vaucouleurs, G. 1983, *ApJS*, 52, 465
- Cellone, S.A., Forte, J.C., & Geisler, D. 1994, *ApJS*, 93, 397
- Choloniewski, J. 1991, *MNRAS*, 250, 486
- Ciotti, L. 1991, *A&A*, 249, 99
- Ciotti, L., & Bertin, G. 1999, 352, 447
- Ciotti, L., Lanzoni, B., & Renzini, A. 1996, *MNRAS*, 282, 1
- Conselice, C.J. *PASP*, 1997, 109, 1251
- Cross, N.J.G., Driver, S.P., Liske, J., Lemon, D.J., Peacock, J.A., Cole, S., Norberg, P., & Sutherland, W.J. 2004, *MNRAS*, 349, 576
- Dalcanton, J.J., & Bernstein, R.A. 2000, *AJ*, 120, 203
- Davies, J.I., Phillipps, S., Boyce, P.J., & Disney, M.J. 1993, *MNRAS*, 260, 491
- Davies, J.I., Phillipps, S., Cawson, M.G.M., Disney, M.J., & Kibblewhite, E.J. 1988, *MNRAS*, 232, 239
- de Grijs, R., Kregel, M., & Wesson, H. 2001, *MNRAS*, 324, 1074
- de Souza, R.E., Gadotti, D.A., & dos Anjos, S. 2004, *ApJS*, 153, 411
- de Vaucouleurs, G. 1948, *Ann. Astrophys.*, 11, 247
- de Vaucouleurs, G. 1956, *Mem. Commonwealth Obs.*, 3, No. 13
- de Vaucouleurs, G. 1959, *Handbuch der Physik*, 53, 275 & 311
- de Vaucouleurs, G. 1977, in *Evolution of Galaxies and Stellar populations*, eds. R. Larson & B. Tinsley (New Haven: Yale University Observatory) p.43
- Disney, M.J., Davies, J.I., & Phillipps, S. 1989, *MNRAS*, 239, 939
- Djorgovski, S., & Spinrad, H. 1981, *ApJ*, 251, 417
- Djorgovski, S., Spinrad, H., & Marr, J. 1984, in *New Aspects of Galaxy Photometry*, J.L.Nieto (ed.), Springer-Verlag
- Doi, M., Fukugita, M., & Okamura, S. 1993, *MNRAS*, 264, 832
- D'Onofrio, M. 2001, *MNRAS*, 326, 1517
- D'Onofrio, M., Capaccioli, M., & Caon, N. 1994, *MNRAS*, 271, 523
- Driver, S.P., Phillipps, S., Davies, J.I., Morgan, I., & Phillipps, S. 1994, *MNRAS*, 266, 155
- Ellis, G.F.R., & Perry, J.J. 1979, *MNRAS*, 187, 357
- Ferrari, F., Dottori, H., Caon, N., Nobrega, A., & Pavani, D.B. 2004, *MNRAS*, 347, 824
- Fraser, C.W. 1972, *The Observatory*, 92, 51
- Graham, A.W. 2001a, *AJ*, 121, 820
- Graham, A.W. 2001b, *MNRAS*, 326, 543
- Graham, A.W. 2004, *ApJ*, 613, L33
- Graham, A.W., & Colless, M.M. 1997, *MNRAS*, 287, 221
- Graham, A.W., Erwin, P., Trujillo, I., & Asensio-Ramos, A. 2003a, in *Carnegie Observatories Astrophysics Series, Vol. 1: Coevolution of Black Holes and Galaxies* (ed. L. C. Ho (Pasadena: Carnegie Observatories, <http://www.ociw.edu/ociw/symposia/series/symposium1/proceedings>))
- Graham, A.W., Erwin, P., Trujillo, I., & Asensio-Ramos, A. 2003b, *AJ*, 125, 2951
- Graham, A.W., & Guzmán, R. 2003, *AJ*, 125, 2936
- Graham, A.W., Lauer, T., Colless, M.M., & Postman, M. 1996, *ApJ*, 465, 534
- Graham, A.W., Trujillo, I., & Caon, N., 2001, *AJ*, 122, 1707
- Graham, A.W., et al. 2005, *AJ*, submitted
- Gunn, J.E., & Oke, J.B. 1975, *ApJ*, 195, 255
- Hoessel, J.G. 1980, *ApJ*, 241, 493
- Infante, I. 1987, *A&A*, 183, 177
- Iodice, E., D'Onofrio, M., Capaccioli, M. 1997, *ASP Conf. Ser.*, 116, 841

- Iodice, E., D'Onofrio, M., Capaccioli, M. 1999, ASP Conf. Ser., 176, 402
- Jones, H., Davies, J.I., & Trewhella, M., 1996, MNRAS, 283, 316
- Karachentseva, V.E., Prugniel, P., Vennik, J., Richter, G.M., Thuan, T.X., & Martin, J.M. 1996, A&ASS, 117, 343
- Kennicutt, R.C. 1989, ApJ, 344, 685
- Khosroshahi, H.G., Wadadekar, Y., & Kembhavi, A. 2000, ApJ, 533, 162
- Kjærgaard, P., Jorgensen, I., & Moles, M. 1993, ApJ, 418, 617
- Kornreich, D.A., Haynes, M.P., & Lovelace, R.V.E. 1998, AJ, 116, 2154
- Kregel, M., & van der Kruit, P.C. 2004, MNRAS, 355, 143
- Kron, R. 1980, ApJS, 43, 305
- Lima Nieto, G.B., Gerbal, D., & Márquez, I. 1999, MNRAS, 309, 481
- MacArthur, L.A., Courteau, S., & Holtzman, J.A. 2003, ApJ, 582, 689
- Marleau, F.R., & Simard, L. 1998, ApJ, 507, 585
- Mazure, A., & Capelato, H.V. 2002, A&A, 383, 384
- Möllenhoff, C., & Heidt, J. A&A, 368, 16
- Morgan, W.W. 1958, PASP, 70, 364
- Morgan, W.W. 1959, PASP, 71, 394
- Morgan, W.W. 1962, ApJ, 135, 1
- Narayan, C.A., & Jog, C.J. 2003, A&A, 407, L59
- Nieto, J.-L., Bender, R., & Surma, P. 1991, A&A, 244, L37
- Okamura, S., Kodaira, K., & Watanabe, M. 1984, ApJ, 280, 7
- Peng, C.Y., Ho, L.C., Impey, C.D., & Hans-Walter, W. 2002, AJ, 124, 266
- Petrosian, V. 1976, ApJ, 209, L1
- Pierini, D., Gordon, K.D., Witt, A.N., & Madsen, G.J. 2004, ApJ, 617, 1022
- Pohlen, M., Dettmar, R., Lutticke, R., & Aronica, G. 2002, A&A, 392, 807
- Pohlen M., Beckman, J.E., Hüttemeister, S., Knapen, J.H., Erwin, P., & Dettmar, R.-J. 2004, in Penetrating Bars Through Masks of Cosmic Dust, eds., D.L. Block, I. Puerari, K.C. Freeman, R. Groess, E.K. Block, A&SS, 319, 713
- Prugniel, P., & Simien, F. 1997, A&A, 321, 111
- Rix, H.-W., & Zaritsky, D. 1995, ApJ, 447, 82
- Rest, A., et al. 2001, AJ, 121, 2431
- Sandage, A., & Perelmuter, J.-M. 1990, ApJ, 350, 481
- Schade, D., Lilly, S.J., Crampton, D., Hammer, F., Le Fevre, O., & Tresse, L. 1995, ApJ, 451, L1
- Seigar, M.S., & James, P.A. 1998, MNRAS, 299, 672
- Sérsic, J.-L. 1963, Boletín de la Asociación Argentina de Astronomía, vol.6, p.41
- Sérsic, J.-L. 1968, Atlas de Galaxias Australes (Córdoba: Observatorio Astronómico)
- Shen, S., et al. 2003, MNRAS, 343, 978
- Trujillo, I., Aguerri, J.A.L., Cepa, J., & Gutiérrez, C.M. 2001a, MNRAS, 321, 269
- Trujillo, I., Aguerri, J.A.L., Cepa, J., & Gutiérrez, C.M. 2001b, MNRAS, 328, 977
- Trujillo, I., Asensio Ramos, A., Rubiño-Martín, J.A., Graham, A.W., Aguerri, J.A.L., Cepa, J., & Gutiérrez, C.M. 2002, MNRAS, 333, 510
- Trujillo, I., Erwin, P., Asensio Ramos, A., & Graham, A.W. 2004, AJ, 127, 1917
- Trujillo, I., Graham, A.W., & Caon, N. 2001c, MNRAS, 326, 869
- Tuffs, R., Popescu, C.C., Volk, H.J., Kylafis, N.D., & Dopita, M.A. 2004, A&A, 419, 821
- van der Kruit, P.C. 1979, A&A, 38, 15
- van der Kruit, P.C. 2001, in Galaxy Disks and Disk Galaxies, G. José, S.J. Funes, E.M. Corsini, ASP Conf. Ser., 230, 119
- van der Kruit, P.C., & Searle, L. 1981, A&A, 95, 105
- Vennik, J., Hopp, U., Kovachev, B., Kuhn, B., & Elsässer, H. 1996, A&ASS, 117, 261
- Vennik, J., & Richter, G.M. Astron. Nachr., 315, H3, 245
- Young, C.K., & Currie, M.J. 1994, MNRAS, 268, L11
- Young, C.K., & Currie, M.J. 1995, MNRAS, 273, 1141